ARTICLE

Supplementary Information

Dual colorimetric-electrochemical microfluidic paper-based analytical device for *point-of-care* testing of ischemic stroke

Silvia Dortez[a†], Marta Pacheco[b†], Teresa Gasull[c], Agustín G. Crevillen[d*], Alberto Escarpa[a,e*]

Table of Contents

1. Dual µPAD design and fabrication

2. Optimization of the electrochemical parameters for Tf detection using dual µPAD

3. Optimization of the colorimetric parameters for Tf-bound iron detection using dual µPAD

4. Electrochemical behavior of anti-Tf-MBs and Tf

5. Stability of the electrochemical detector of the dual µPAD

6. Assessment of TSAT in serum samples from ischemic stroke patients by using the dual µPAD

7. General characteristics of dual PADs combining colorimetry and electrochemical detection for the determination of analytes of clinical relevance

8. References

[a] *Department of Analytical Chemistry, Physical Chemistry and Chemical Engineering, University of Alcala, 28805, Alcala de Henares, Madrid, Spain.*
[b] *Department of Chemistry in Pharmaceutical Sciences, Analytical Chemistry, Faculty of Pharmacy, Complutense University of Madrid, 28040 Madrid, SpainAddress here.*
[c] *Cellular and Molecular Neurobiology Research Group, Department of Neurosciences, Germans Trias i Pujol Research Institute (IGTP), 08916, Badalona, Barcelona, Spain.*
[d] *Department of Analytical Sciences, Faculty of Sciences, Universidad Nacional de Educación a Distancia (UNED), 28040, Madrid, Spain.*
[e] *Chemical Research Institute "Andrés M. Del Río" (IQAR), University of Alcala, 28805, Alcala de Henares, Madrid, Spain.*

*Corresponding authors:
Alberto Escarpa, Department of Analytical Chemistry, Physical Chemistry and Chemical Engineering and Chemical Research Institute "Andres M. Del Rio", Universidad de Alcalá, Madrid, Spain (alberto.escarpa@uah.es)
Agustín G. Crevillen, Department of Analytical Sciences, Faculty of Sciences, Universidad Nacional de Educación a Distancia (UNED), Madrid, Spain (agustingcrevillen@ccia.uned.es)

† Both authors contributed equally.

Electronic Supplementary Information (ESI) available: [details of any supplementary information available should be included here]. See DOI: 10.1039/x0xx00000x

ARTICLE

1. Dual µPAD design and fabrication

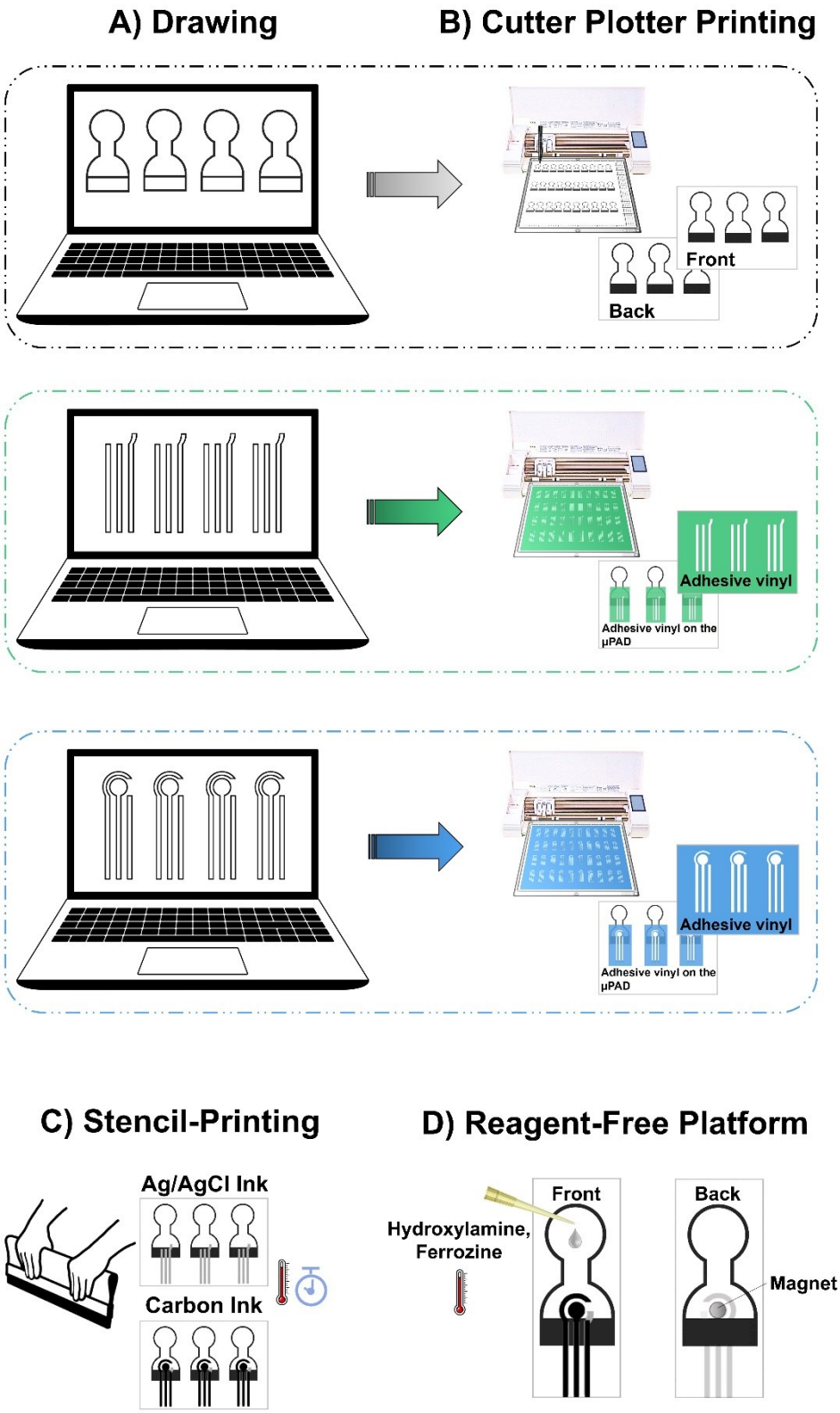

Fig. S1. Schematic representation of the fabrication of the dual colorimetric-electrochemical µPAD (drawing, stencil-printing, and reagent-free platform).

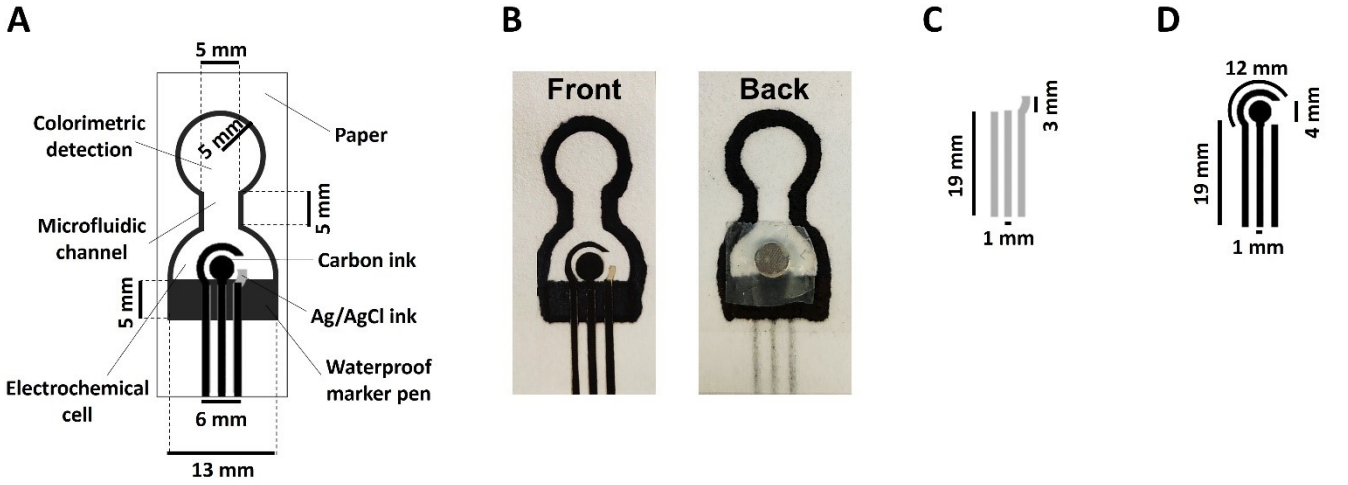

Fig. S2. (A) Dimensions of the dual colorimetric-electrochemical µPAD for reagent-free detection and quantification of TSAT in serum samples. (B) Image of a dual colorimetric-electrochemical µPAD. (C) Ag/AgCl ink pattern. (D) Carbon ink pattern.

2. Optimization of the electrochemical parameters for Tf detection using dual µPAD

To achieve the best analytical performance of the dual µPADs for Tf detection, several components and parameters were optimized. All experiments were performed in triplicate.

Initially, different carbon inks from different commercial companies (SunChemical and Henkel) were tested for the manufacture of µPADs and compared with commercial SPCEs. The two types of inks used in the µPADs and the control (SPCE DRP-110) were characterized by electrochemical impedance spectroscopy (EIS) and by cyclic voltammetry (CV), using 5 mM $K_4Fe(CN)_6/K_3Fe(CN)_6$ in 0.1 M KCl electrolyte as redox probe (ferro/ferri system), to evaluate their electrochemical performance (Fig. S3). Fig. S3A shows cyclic voltammograms of the ferro/ferri system for each carbon ink. It can be seen that the µPAD fabricated with carbon ink from SunChemical shows better reversibility (least difference between the anodic peak potential and the cathodic peak potential) than the rest of the disposable devices, which means a faster electron transfer, and highest peak currents compared to other carbon inks. Fig. S3B shows the EIS results for each type of electrode using the ferro/ferri system, where the lowest heterogeneous charge transfer resistance is experienced by the µPAD fabricated with carbon ink from SunChemical (which coincides with the results obtained by CV). Based on both studies, clearly the µPAD fabricated with carbon ink from SunChemical showed the best electrochemical behavior. Therefore, it was chosen to manufacture all dual µPADs for the rest of the experiments. Then different depositions of Ag/AgCl and carbon ink layers were evaluated by CV with 5 mM ferro/ferri system. 1 layer of Ag/AgCl + 1 layer of carbon ink, 1 layer of Ag/AgCl + 2 layers of carbon ink, 2 layers of Ag/AgCl + 1 layer of carbon ink, and 2 layers of Ag/AgCl + 2 layers of carbon ink were tested (Fig. S3C). With the deposition of one layer of Ag/AgCl ink and one layer of carbon ink (Fig. S3C, black line) the best reversibility and highest peak currents were obtained compared to the other layer depositions, so it was chosen to perform the stencil-printing of the dual µPADs.

Following the optimization studies, different operational conditions were tested for electrochemical detection. Volumes of 20, 30, and 50 µL of 5 mM ferro/ferri system were added to the µPAD and evaluated electrochemically by CV comparing anodic peak currents (Fig. S4A). 30 µL of solution was chosen as the optimal volume (Fig. S4A, red line) because it was able to fully impregnate the dual µPAD and cover the electrochemical cell to obtain high sensitivity in the measurements. 20 µL showed low anodic peak current and 50 µL showed the same sensitivity as 30 µL but the device leaked due to the high volume.

Next, the appropriate electrochemical technique was chosen for the Tf detection. For this, the voltammetric measurement was carried out both by square wave voltammetry (SWV) and by differential pulse voltammetry (DPV) with 30 µL of 5 g L^{-1} Tf solution

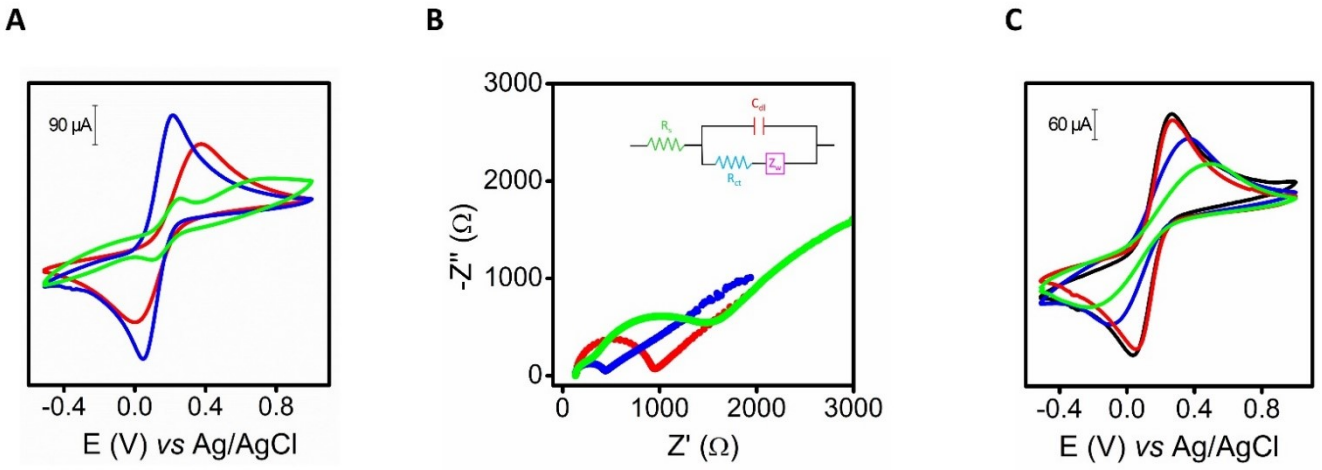

(in 0.2 M BR buffer pH 3.0) under the same experimental conditions. A sensitivity (peak height at +0.8 V) 10-folds greater was obtained by SWV than by DPV (Fig. S4B), so SWV was the electrochemical technique used for the analysis of Tf.

Fig. S3. (A) CV of SPCE (red line), µPAD with carbon ink from SunChemical (blue line), and µPAD with carbon ink from Henkel (green line) of 5 mM $K_4Fe(CN)_6/K_3Fe(CN)_6$ in 0.1 M KCl electrolyte as redox probe. CV parameters: start potential –0.5 V, end potential +1.0 V, scan rate 0.1 V s^{-1} (n = 3). (B) Nyquist plots corresponding to SPCE (red line), µPAD with carbon ink from SunChemical (blue line), and µPAD with carbon ink from Henkel (green line) of 5 mM $K_4Fe(CN)_6/K_3Fe(CN)_6$ in 0.1 M KCl electrolyte as redox probe. EIS parameters: frequencies ranged from 100,000 to 0.01 Hz (n = 3). (C) CV of different depositions of Ag/AgCl and carbon ink layers in the µPAD of 5 mM $K_4Fe(CN)_6/K_3Fe(CN)_6$ in 0.1 M KCl electrolyte as redox probe. 1 layer of Ag/AgCl + 1 layer of carbon ink (black line), 1 layer of Ag/AgCl + 2 layers of carbon ink (blue line), 2 layers of Ag/AgCl + 1 layer of carbon ink (red line), and 2 layers of Ag/AgCl + 2 layers of carbon ink (green line). CV parameters: see Fig. S3A (n = 3).

The following study was the optimization of the analysis frequency in the SWV technique for the detection of Tf. Frequencies of 50, 100, 200, 300, and 400 Hz were evaluated (Fig. S4C). Frequencies of 50 and 100 Hz showed low signal at + 0.8 V compared to the higher frequencies. No significant differences were obtained between 200, 300, and 400 Hz in terms of peak current, only broadening of the signal, so 200 Hz was chosen as the optimal parameter due to its good resolution and peak current at + 0.8 V using 5 g L^{-1} Tf in 0.2 M BR buffer pH 3.0.

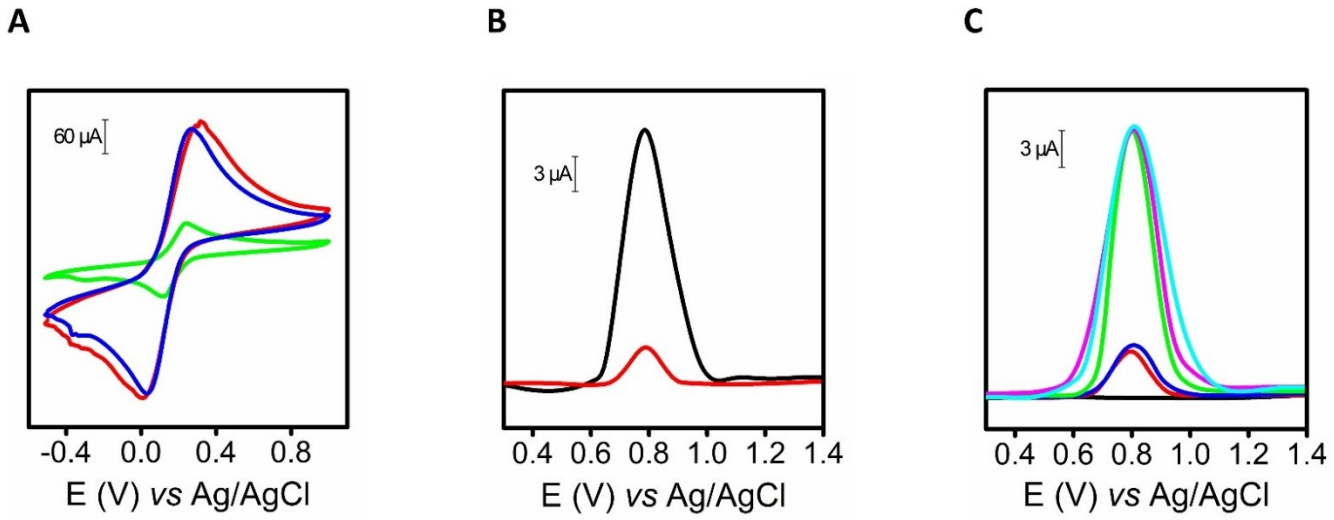

Fig. S4. (A) CV of different volumes of 5 mM $K_4Fe(CN)_6/K_3Fe(CN)_6$ in 0.1 M KCl electrolyte added on the µPAD. 20 µL of ferro/ferri system (green line), 30 µL of ferro/ferri system (red line), and 50 µL of ferro/ferri system (blue line). CV parameters: see Fig. S3A (n = 3). (B) Comparison between different electrochemical techniques. SWV of 30 µL of 5 g L^{-1} Tf in 0.2 M BR buffer pH 3.0 (black line) and DPV of 30 µL of 5 g L^{-1} Tf in 0.2 M BR buffer pH 3.0 (red line). SWV parameters: start potential +0.3 V, end potential +1.4 V, frequency 200 Hz, amplitude 0.05 V, and step potential 0.005 V. DPV parameters: start potential +0.3 V, end potential +1.4 V, modulation time 0.005 s, amplitude 0.05 V, and step potential 0.005 V (the

background signal was linearized) (n = 3). (C) Comparison between different frequencies in the SWV technique. Voltammograms corresponding to 30 µL of 0.2 M BR buffer pH 3.0 (black line), and 5 g L^{-1} Tf at 50 Hz (red line), at 100 Hz (blue line), at 200 Hz (green line), at 300 Hz (purple line), and at 400 Hz (cyan line). Rest of SWV parameters: see Fig. S4B (the background signal was linearized) (n = 3).

Next, the solution and the pH of the electrolyte used for the Tf determination in serum samples was also optimized, since it can affect the electrochemical and colorimetric measurements. As mentioned above, an acidic medium is necessary for the release of Tf-bound iron (see section *Immunopurification step for Tf isolation and Tf-bound iron release in serum samples* of the main text). In previous works by our research group [1,2], we used 2 M acetate buffer pH 4.8 as electrolyte solution. For the electrochemical measurement of Tf standard solution, 2 M acetate buffer pH 4.8 showed high sensitivity because the acid pH was close to its isoelectric point; however, the studies with human serum samples revealed very low peak currents of Tf, probably due to the high ionic strength of the electrolyte. Therefore, 0.2 M BR buffer pH 3.0 was used as an electrolyte solution for the electrochemical detection of Tf, providing high sensitivity in the analysis (Fig. S5A) and being capable of fully releasing Tf-bound iron both standard solutions (Tf and Fe^{3+}) and in human serum samples.

Finally, to demonstrate that there is no cross-interference between both detection modes (between the analytes Tf and Fe^{3+}), different controls were performed to verify the electrochemical behavior of Fe^{3+} and Tf. As can be observed in Fig S5B, there is no peak neither for a standard solution of 70 µg mL^{-1} Fe^{3+} (the highest concentration in calibration plot, red line) nor 0.2 M BR buffer pH 3.0 (black line), compared to the peak at +0.8 V of 0.25 g L^{-1} Tf (the lowest concentration in calibration plot, blue line), using the dual µPAD designed in this work based exclusively on carbon ink.

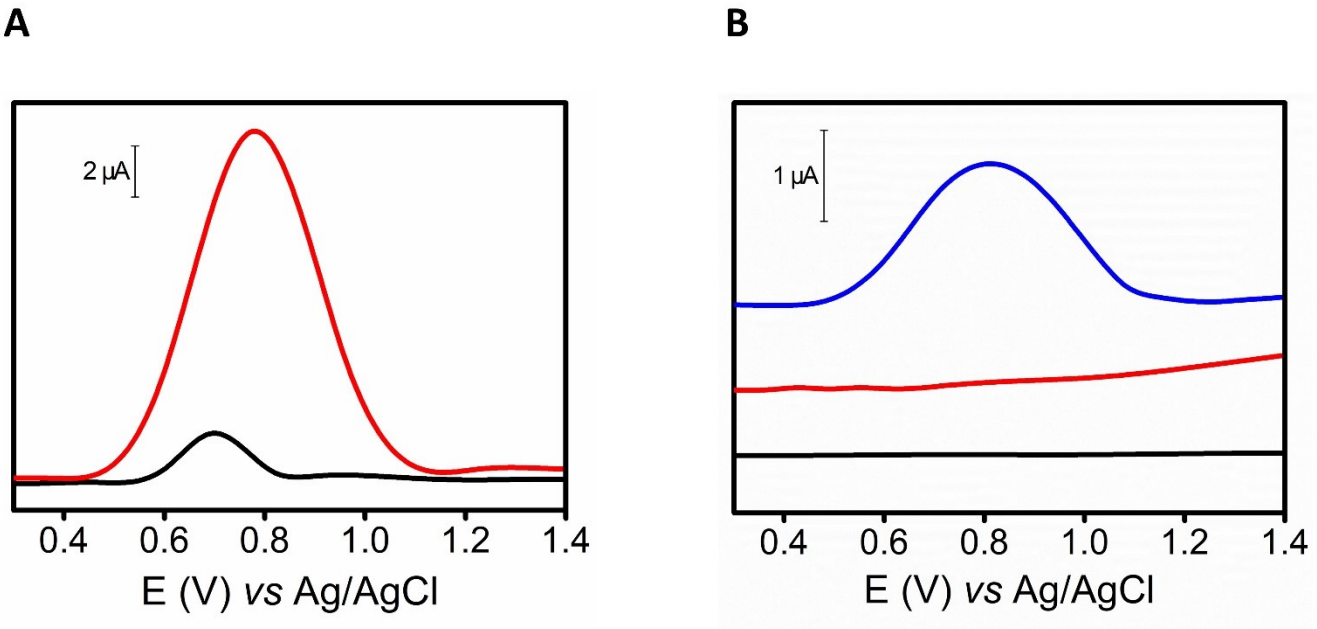

Fig. S5. (A) Comparison between different acidic medium for Tf determination from a serum sample after the immunopurification step. Voltammograms corresponding to 30 µL of Tf-anti-Tf-MBs in 2 M acetate buffer pH 4.8 (black line) and Tf-anti-Tf-MBs in 0.2 M BR buffer pH 3.0 (red line). (B) SWV of 30 µL of 0.2 M BR buffer pH 3.0 (black line), 70 µg mL^{-1} Fe^{3+} in 0.2 M BR buffer pH 3.0 (red line), and 0.25 g L^{-1} Tf in 0.2 M BR buffer pH 3.0 (blue line). SWV parameters: see Fig. S4B (the background signal was linearized) (n = 3).

3. Optimization of the colorimetric parameters for Tf-bound iron detection using dual µPAD

To obtain a reagent-free device, several analytical parameters were optimized by measuring the color intensity formed in the colorimetric detection reservoir of dual µPADs after the addition of Fe^{3+} standard solutions. All experiments were performed in triplicate. For colorimetric detection, the electrolyte solution used to prepare the hydroxylamine and ferrozine solutions is 2 M acetate buffer pH 4.8.

Different volumes of 100 mg mL^{-1} hydroxylamine (in 2 M acetate buffer pH 4.8), namely 1, 5, 10, and 30 µL, were added into the circular colorimetric detection reservoir and the µPADs were fully dried in an oven at 60 ºC for 2 min. Next, the colorimetric detection reservoir of the dual µPADs was impregnated with 0.5 µL of 49 mg mL^{-1} ferrozine (in 2 M acetate buffer pH 4.8) and the

µPADs were fully dried in an oven at 60 ºC for 2 min. Finally, 30 µL of 20 µg mL^{-1} Fe^{3+} standard solution (in 0.2 M BR buffer pH 3.0) was added to the electrochemical reservoir of the dual µPAD and allowed to flow through the microfluidic channel to the colorimetric detection reservoir, where the reduction from Fe^{3+} to Fe^{2+} occurs by the reducing agent hydroxylamine, and the subsequent formation of the colored Fe^{2+}–ferrozine complex (2 min reaction time). As reported in Fig. S6A, a significant increase in color intensity was obtained from 1 to 30 µL of 100 mg mL^{-1} hydroxylamine. To be sure that all Fe^{3+} was reduced to Fe^{2+}, the color intensity obtained by the reagent-free µPAD (30 µL of 100 mg mL^{-1} hydroxylamine preloaded) was also compared with that obtained by a 30 µL of 20 µg mL^{-1} Fe^{3+} standard solution in 100 mg mL^{-1} hydroxylamine solution (reduction performed out of the µPAD with an excess of hydroxylamine) added to the device (last bar of Fig. S6A). No significant differences were obtained between both strategies, so the Fe^{3+} reduction was completed. Therefore 30 µL was selected as the optimal volume.

However, 30 µL is a very high volume capable of covering the entire µPAD and, therefore, may affect the electrochemical measurement because the effective electrode surface in contact with the solution is that touching the paper, rather than the electrode surface at the air interface. When measuring 5 g L^{-1} Tf (in 0.2 M BR buffer pH 3.0) by SWV in a reagent-free µPAD loaded with 30 µL of hydroxylamine (Fig. S6B, green line), no peak was obtained at +0.8 V since a high anodic current intensity was observed that corresponded to the same voltammogram obtained in a 100 mg mL^{-1} hydroxylamine solution (in 2 M acetate buffer pH 4.8) (Fig. S6B, blue line), which negatively impacts the detection of Tf in serum samples. To solve this problem, three depositions of 10 µL (3 x 10 µL) of 100 mg mL^{-1} of hydroxylamine (in 2 M acetate buffer pH 4.8) were performed, with prior drying in an oven at 60 ºC for 2 min between each reagent addition, since 10 µL were capable of covering the entire colorimetric detection reservoir and the microfluidic channel without coming into contact with the electrochemical cell. The color intensity obtained by this strategy was equal to that provided by one drop of 30 µL (see Fig. S6A). For this reason, 3 x 10 µL of 100 mg mL^{-1} of hydroxylamine (in 2 M acetate buffer pH 4.8) was selected as the optimal volume for the formation of a reagent-free dual µPAD.

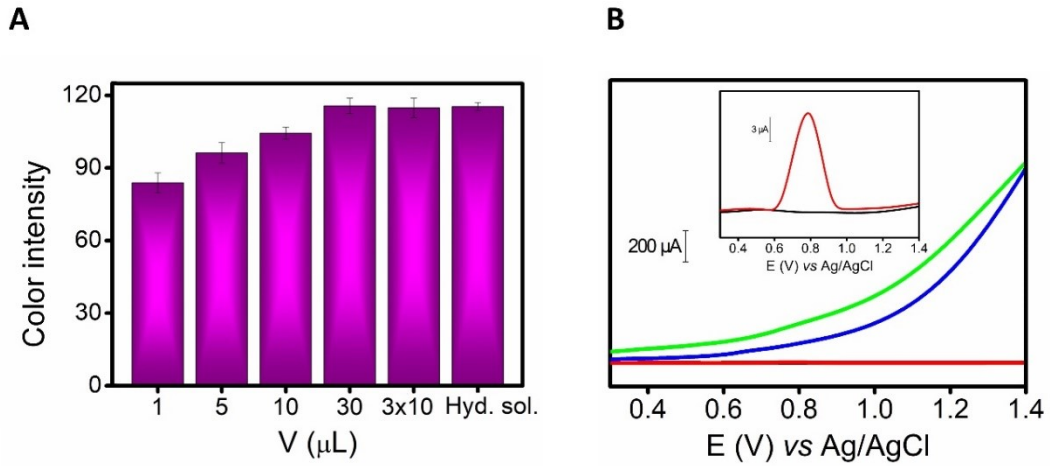

Fig. S6. (A) Color intensity (green channel) at different 100 mg mL^{-1} hydroxylamine solution (in 2 M acetate buffer pH 4.8) volumes added in the dual µPAD and its comparison with 20 µg mL^{-1} of Fe^{3+} standard solution in 100 mg mL^{-1} of hydroxylamine solution (in 2 M acetate buffer pH 4.8) for the formation of the Fe^{2+}–ferrozine complex. Experimental conditions: 0.5 µL of 49 mg mL^{-1} ferrozine in 2 M acetate buffer pH 4.8 and 30 µL of 20 µg mL^{-1} Fe^{3+} standard solution in 0.2 M BR buffer pH 3.0. 2 min reaction time (n = 3). (B) SWV of 30 µL of 0.2 M BR buffer pH 3.0 (black line), 5 g L^{-1} Tf in 0.2 M BR buffer pH 3.0 (red line), 100 mg mL^{-1} hydroxylamine solution in 2 M acetate buffer pH 4.8 (blue line), and 30 µL of 5 g L^{-1} Tf in 0.2 M BR buffer pH 3.0 + 30 µL of 100 mg mL^{-1} hydroxylamine in 2 M acetate buffer pH 4.8 added in the dual µPAD (green line). Inset: Rescaling of the voltammogram provided by 5 g L^{-1} Tf in 0.2 M BR buffer pH 3.0. SWV parameters: see Fig. S4B (n = 3).

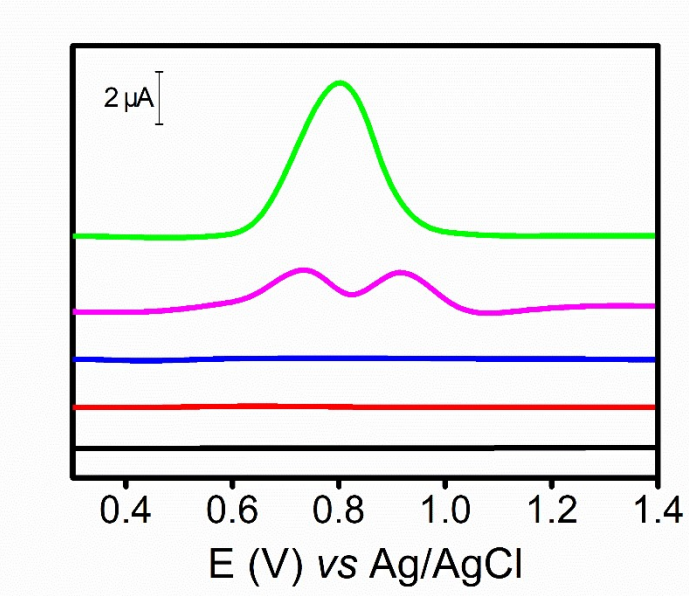

4. Electrochemical behavior of anti-Tf-MBs and Tf

Fig. S7. Voltammograms obtained by SWV of 30 µL of 0.2 M BR buffer pH 3.0 (blank) (black line), MBs in 0.2 M BR buffer pH 3.0 (control) (red line), anti-Tf-MBs in 0.2 M BR buffer pH 3.0 (control) (blue line), 7.5 µg mL^{-1} of anti-Tf in 0.2 M BR buffer pH 3.0 (control) (purple line), and Tf-anti-Tf-MBs in 0.2 M BR buffer pH 3.0 (green line) from a commercial serum sample after the immunopurification step without preconcentration. SWV parameters: see Fig. S4B (the background signal was linearized) (n = 3).

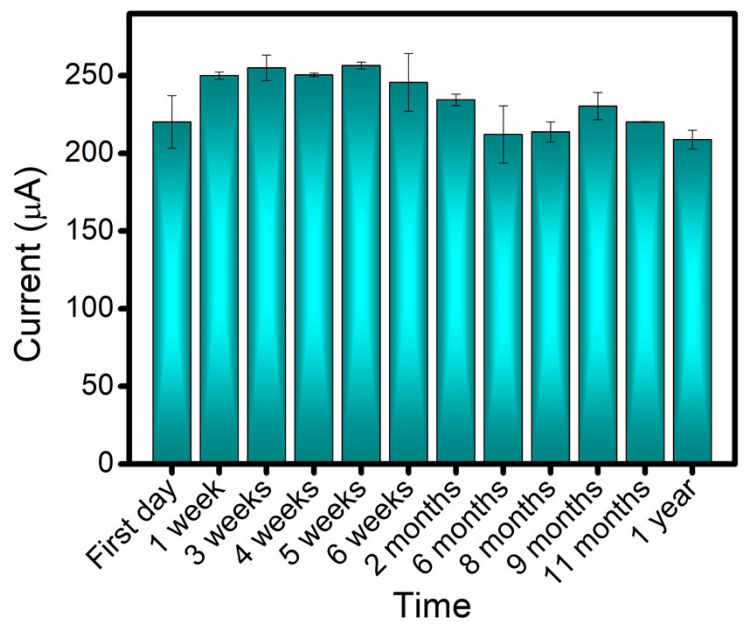

5. Stability of the electrochemical detector of the dual µPAD

Fig. S8. Stability of the electrochemical detector of the dual μPAD (in plastic zipper bags at room temperature and in a dark) with a 5 mM $K_4Fe(CN)_6/K_3Fe(CN)_6$ in 0.1 M KCl system solution evaluated by CV. CV parameters: see Fig. S3A (n = 3).

6. Assessment of TSAT in serum samples from ischemic stroke patients by using the dual μPAD

Table S1. TSAT in serum samples from ischemic stroke patients obtained by dual μPAD and by urea-PAGE (n = 3).

Sample	$TSAT_{dual\ \mu PAD}$ (%)	$TSAT_{urea\text{-}PAGE}$ (%)[3]
S1	17 ± 2	15 ± 3
S2	17 ± 1	18 ± 4
S3	20 ± 2	21 ± 1
S4	34 ± 3	33 ± 7
S5	35 ± 2	34 ± 7
S6	36 ± 6	35 ± 3
S7	45 ± 6	38 ± 4
S8	40 ± 3	40 ± 3
S9	42 ± 5	46 ± 1

7. General characteristics of dual PADs combining colorimetry and electrochemical detection for the determination of analytes of clinical relevance

Table S2. Dual PAD with colorimetric (CD) and electrochemical (ED) detection applied in the clinical fields.

Analytes (Detection)	Integrated detection into the same PAD	Samples	Application	Ref. Main Text	Ref. SI
Thiocyanate (CD & ED)	Yes	Saliva	Tobacco consumption	66	4
MCF-7 cells (CD & ED)	Yes	Spiked serum	Cancer diagnosis	67	5
Uracil-DNA glycosylase (CD & ED)	No	A549 Cell culture	DNA damage	68	6
Glucose (CD & ED)	No	Serum	Monitoring blood sugar	69	7
Nitrite, pH, α-amylase (CD) / Lactate (ED)	Yes*	Saliva	Periodontitis diagnosis	70	8

Fe^{3+} (CD) / Transferrin (ED)	Yes*	Serum	Ischemic stroke	This work	This work

*Unique dual µPAD works with detection of more than one analyte integrated into a single device.

8. References

1 S. Dortez, A. G. Crevillen and A. Escarpa, *Talanta*, 2023, **253**, 123914.
2 S. Dortez, N. DeGregorio-Rocasolano, M. Millán, T. Gasull, A. G. Crevillen and A. Escarpa, *Anal. Chem.*, 2023, **95**, 12391−12397.
3 N. DeGregorio-Rocasolano, O. Martí-Sistac, J. Ponce, M. Castelló-Ruiz, M. Millán, V. Guirao, I. García-Yébenes, J. B. Salom, P. Ramos-Cabrer, E. Alborch, I. Lizasoain, J. Castillo, A. Dávalos and T. Gasull, *Redox Biol.*, 2018, **15**, 143–158.
4 K. Pungjunun, A. Yakoh, S. Chaiyo, N. Praphairaksit, W. Siangproh, K. Kalcher and O. Chailapakul, *Microchim. Acta*, 2021, **188**, 1-11.

5 H. Wang, C. Zhou, X. Sun, Y. Jian, Q. Kong, K. Cui, S. Ge and J. Yu, *Biosens. Bioelectron*., 2018, **117**, 651-658.
6 W. Xue, P. Jia, Y. Wu, P. Wang, J. Shi, Y. Chan and M. Liu, *Adv. Agrochem.*, 2023, **2**, 269-275.
7 J. Xu, J. Shen, B. Zhang, Y. Zhang, X. Lv and G. Zhu, *Electrochim. Acta*, 2024, **481**, 143952.
8 L. R. Sousa, H. A. Silva-Neto, L. F. Castro, K. A. Oliveira, F. Figueredo, E. Cortón and W. K. T. Coltro, *Anal. Bioanal. Chem.*, 2023, **415**, 4391-4400.